View metadata, citation and similar papers at core.ac.uk
brought to you by CORE
provided by Infoscience - École polytechnique fédérale de Lausanne

Bel Hadj Ali, N. and Smith, I.F.C. "Dynamic behavior and vibration control of a tensegrity structure", International Journal of Solids and Structures, Vol.47, No.9, 2010, pp 1285-1296. doi:10.1016/j.ijsolstr.2010.01.012

Dynamic behavior and vibration control of a tensegrity structure

N. Bel Hadj Ali* and I.F.C. Smith

Applied Computing and Mechanics Laboratory
Ecole Polytechnique Fédérale de Lausanne (EPFL)
ENAC/IS/IMAC, Station 18, 1015 Lausanne, Switzerland

Abstract

Tensegrities are lightweight space reticulated structures composed of cables and struts. Stability is provided by the self-stress state between tensioned and compressed elements. Tensegrity systems have in general low structural damping, leading to challenges with respect to dynamic loading. This paper describes dynamic behavior and vibration control of a full-scale active tensegrity structure. Laboratory testing and numerical simulations confirmed that control of the self-stress influences the dynamic behavior. A multi-objective vibration control strategy is proposed. Vibration control is carried out by modifying the self-stress level of the structure through small movement of active struts in order to shift the natural frequencies away from excitation. The PGSL stochastic search algorithm successfully identifies good control commands enabling reduction of structural response to acceptable levels at minimum control cost.

Keywords: Tensegrity, Structural dynamics, Vibration control, Multi-objective optimization

1. Introduction

Tensegrities are spatial, reticulated and lightweight structures that are composed of struts and tendons. Stability is provided by the self-stress state between tensioned and compressed elements. A widely accepted definition has been proposed by Motro (2003): "*A tensegrity is a system in stable self-equilibrated state comprising a discontinuous set of compressed components inside a continuum of tensioned components"*. Tensegrities have received significant interest among scientists and engineers in fields such as architecture, civil engineering and aerospace applications. Among different traditional approaches, the tensegrity concept is one of the most promising for active and deployable structures. When used for structural applications, tensegrity systems might be subjected to dynamic loading such as those caused by wind, impact or earthquakes. Being lightweight structures, tensegrities are particularly sensitive to dynamic loading and thus likely to present significant vibration levels.

In spite of much research related to geometry, form-finding and architecture of tensegrity structures, few studies have focused on dynamic behavior. In the mid 1980s, Motro performed dynamic experimental and numerical work on a tensegrity structure composed of three bars and 9 tendons (Motro et al. 1986). Motro showed that a linearized dynamic model around an equilibrium configuration offers a good approximation of the nonlinear behavior of simple tensegrity structures. Furuya (1992) examined the vibrational

characteristics of a tensegrity mast and showed that the modal frequencies increase as the pretension increases. Kono et al. (1999) experimentally investigated a 9m span double-layer tensegrity grid subjected to dynamic loading. Ben Kahla et al. (2000) developed a numerical procedure for nonlinear dynamic analysis of tensegrity systems. Murakami (2001a; 2001b) used Lagrangian and Eulerian approach to derive the equations of motion of tensegrity structures and performed numerical simulations and modal analysis of some tensegrity modules. Oppenheim and Williams (2001a; 2001b) examined the dynamic behavior of a simple elastic tensegrity structure. They showed that the natural damping of the tensegrity elements is poorly mobilized due to the existence of infinitesimal mechanisms. Sultan et al. (2002) derived linearized dynamic models for two classes of tensegrity structures and showed that the modal dynamic range generally increases with the pretension. Carstens and Kuhl (2005) performed nonlinear dynamic analysis of a tensegrity tower using discontinuous and continuous Galerkin time integration schemes. Arsenault and Gosselin (2006) developed dynamic models of planar tensegrity modules with 1, 2 and 3 degrees of freedom. Masic and Skelton (2006) used a linearized dynamic model to enhance the dynamic control performance of a tensegrity structure. Dubé et al. (2008) presented a comparative study between experimental tests and numerical simulations carried out on a tensegrity minigrid considering static as well as dynamic loading. Recently, Tan and Pellegrino (2008) investigated the nonlinear vibration of a cable-stiffened pantographic deployable structure and showed that the system resonant frequencies are related to the level of active cable pretension. All studies cited so far aimed to find a dynamic model of tensegrity structures and to predict their behavior. Most studies are either analytical or numerical, rarely both. Also, experimental studies rarely included full-scale structures.

Research into active control of tensegrity structure was initiated in the mid 1990s. Tensegrities are attractive solutions for controllable and smart structures as often, small amounts of energy are needed to change the shape of tensegrity structures (de Jager and Skelton 2005). Experimental work that explored the active tensegrity potential was carried out by Fest et al. (2004) on a five-module active tensegrity structure. A quasi-static control strategy based on stochastic search is first proposed to satisfy serviceability criterion (Domer and Smith 2005). The control strategy is then extended to take into account additional robustness objectives (Adam and Smith 2007b). Djouadi et al. (1998) developed an active control algorithm for vibration damping of tensegrity structures intended to spatial applications. Kanchanasaratool and Williamson (2002) used a nonlinear constrained particle method to develop a dynamic model for a general class of tensegrity structures. This model is then used to investigate feedback shape control for a tensegrity module with three actuated bars and nine passive strings. Chan et al. (2004) presented an experimental study of active vibration control of a three-stage tensegrity structure. Active damping is performed using local integral force feedback and acceleration feedback control. Although performed on a small scale tensegrity structure, experiments showed that the control procedure gives significant damping for the first 2 resonance bending modes. Averseng and Crosnier (2004) introduced a vibration control approach based on robust control. They presented experimental validation done with a tensegrity plane grid of 20 m^2 where an actuation system is connected to the supports. de Jager and Skelton (2005) have

investigated placement of sensors and actuators to control vibrations on a planar tensegrity structure made up of three units. Ganesh Raja and Narayanan (2007) presented a theoretical analysis of vibration control of a two module tensegrity structure under random excitations using optimal control theory and where control is performed by means of piezoelectric actuators.

Few experimental studies have been observed to be of practical significance. Results are mainly tested numerically on small, simple and symmetrical tensegrity models. Neither experimental modal identification nor testing under dynamic loads for multiple self-stress levels could be found in the literature. Structures are much simpler than would be needed for practical applications. Furthermore, no study has examined attenuation of dynamic vibrations using active control of a large scale tensegrity structure.

This paper extends ten years of research work on quasi-static control to perform dynamic analyses and study vibration control of a full-scale active tensegrity structure. Resonance modes of the structure are identified experimentally and compared with those determined through a finite element model. Dynamic behavior of the tensegrity structure is experimentally identified through testing under dynamic excitation. Laboratory testing is carried out for multiple self-stress levels and for different excitation frequencies. The dynamic behavior of the structure is also numerically simulated. Vibration control is then carried out by modifying the self-stress level of the structure through contractions and elongations of active struts in order to shift the natural frequencies away from excitation. Stochastic search is used to identify good control commands enabling reduction of structural response to acceptable levels at minimum control cost.

2. Description of active tensegrity structure

The structure that is used for experimental testing is composed of 5 modules and rests on three supports (Fig. 1). It covers a surface area of $15m^2$, has a height of 1.20m and has a distributed dead load of $300N/m^2$. It is composed of 30 struts and 120 tendons. Struts are fiber reinforced polymer tubes with a modulus of elasticity of 28GPa and a specific mass of $2420kg/m^3$. With a diameter of 60mm and a cross-section area of $703mm^2$, the ultimate buckling load for these elements is estimated to be 42kN. Tendons are stainless steel cables, with a modulus of elasticity of 115GPa and a cross-section area of $13.85mm^2$. In each module, struts converge toward a central node where connection is provided by contact compression in a steel ball. This topology was proposed to limit buckling lengths, thereby allowing for more slender compression elements than more traditional tensegrities (Paronesso and Passera 2004). The structure rests on three supports that allow statically determinate support conditions. The structure is also equipped with ten active struts placed in in-line pairs in each module. Actuated struts are used for strut length adjustment controlling by the way the self-stress state in the tensegrity structure (Fig. 2). Vertical displacements of ten nodes of the top surface edge of the structure are measured with inductive displacement sensors (Fig. 3). A more detailed description of the structure and the active control system is provided in (Adam 2007) and (Fest et al. 2004) .

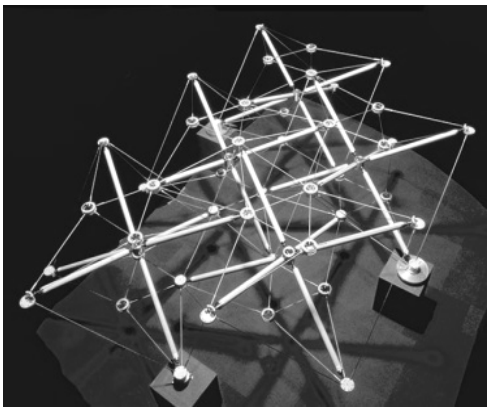

Fig. 1. Five module, tensegrity structure

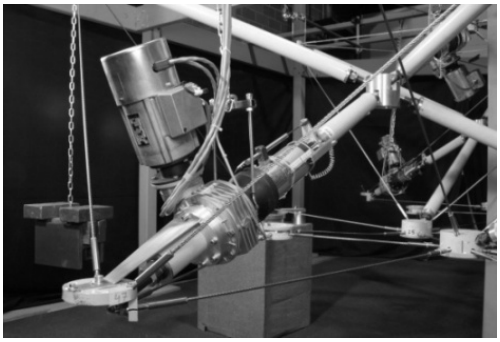

Fig. 2. One of the ten active struts of the tensegrity structure

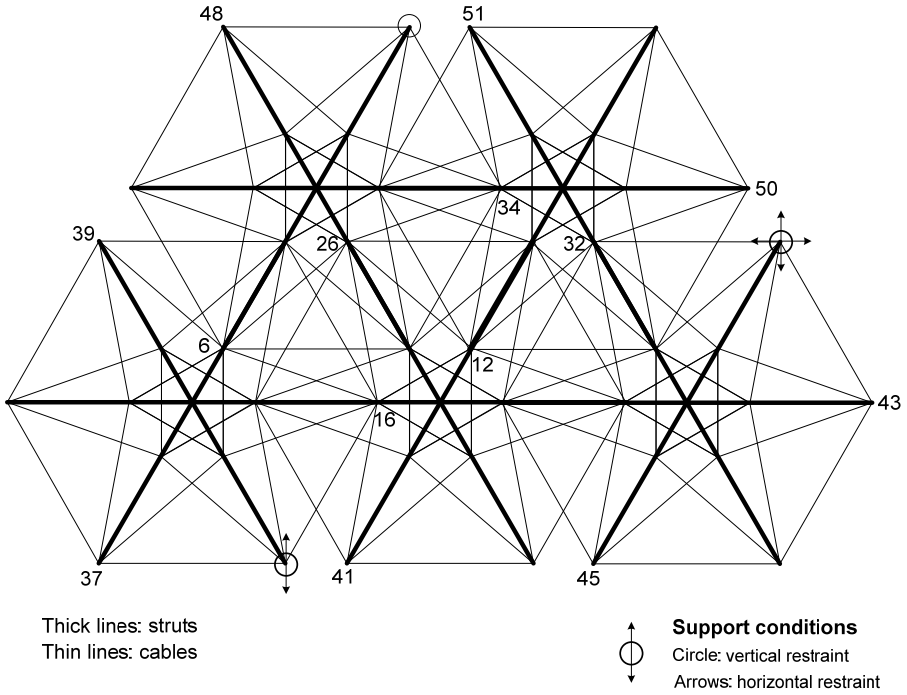

Fig. 3. View of the structure from above with numbering of nodes of the top surface

3. Analytical formulation

Tensegrity systems are a special class of spatial and reticulated structures. The stability of these structures is provided by the self-stress state between tensioned and compressed members. Tensegrity systems are closely coupled structures that display geometrically non-linear behavior and require specialized analysis techniques even under static loading (Barnes 1999; Domer et al. 2003; Kebiche et al. 1999). Research over the last decades has resulted in several linear and nonlinear models describing the dynamic behavior of tensegrity structures (Mirats Tur and Juan 2009). Motro et al (1986) showed that the equation of motion linearized at a pre-stressed configuration can be efficiently used instead of a complete nonlinear dynamic model. This simplified approach was first used to investigate the dynamic behavior of simple tensegrity modules and then extended to more complex configurations (Murakami and Nishimura 2001a; Sultan et al. 2002).

A linearized dynamic model written around an equilibrium configuration is used to describe the dynamic behavior of the active tensegrity structure. The linearized equation of motion at a pre-stressed configuration is as follow:

$$\boldsymbol{M}\ \ddot{u} + \boldsymbol{C}\ \dot{u} + \boldsymbol{K_T}\ u = \boldsymbol{F} \qquad \text{[Eq. 1]}$$

Where: $\boldsymbol{M}$, $\boldsymbol{C}$ and $\boldsymbol{K_T}$ are the mass, damping and tangent stiffness matrices, respectively. $\boldsymbol{F}$ is the applied load vector. u, $\dot{u}$ and $\ddot{u}$ are respectively vectors of nodal displacement, velocity and acceleration. The tangent stiffness matrix $\boldsymbol{K_T}$ is decomposed into the linear stiffness matrix $\boldsymbol{K_E}$, commonly used for small-deformation truss analyses, and the geometrical stiffness matrix $\boldsymbol{K_G}$ induced by self-stresses (Guest 2006).

$$\boldsymbol{K_T} = \boldsymbol{K_E} + \boldsymbol{K_G} \qquad \text{[Eq. 2]}$$

For the development of a finite element model of the tensegrity structure, each element in the structure is characterized by the following mass and stiffness matrices (Kebiche et al. 1999):

$$\boldsymbol{K_E} = \left(\frac{EA}{L}\right).\begin{bmatrix} I_0 & -I_0 \\ -I_0 & I_0 \end{bmatrix} \qquad \text{[Eq. 3]}$$

$$\boldsymbol{K_G} = \left(\frac{T}{L}\right).\begin{bmatrix} I_3 & -I_3 \\ -I_3 & I_3 \end{bmatrix} \qquad \text{[Eq. 4]}$$

$$\boldsymbol{M} = \left(\frac{m}{6}\right).\begin{bmatrix} 2I_3 & -I_3 \\ -I_3 & 2I_3 \end{bmatrix} \qquad \text{[Eq. 5]}$$

$$I_0 = \begin{bmatrix} 1 & 0 & 0 \\ 0 & 0 & 0 \\ 0 & 0 & 0 \end{bmatrix} \qquad \text{[Eq. 6]}$$

$$I_3 = \begin{bmatrix} 1 & 0 & 0 \\ 0 & 1 & 0 \\ 0 & 0 & 1 \end{bmatrix} \qquad \text{[Eq. 7]}$$

Where: E is the elastic modulus; A is the member area; L is the length of the member and T is the axial load. Mass and stiffness matrices are first formulated in a local coordinate system {*xyz*} where *x* is along the element axis. The global mass and stiffness matrices **M** and $\mathbf{K_T}$ are obtained by adding up contributions from the individual elements expressed in a global coordinate system {XYZ}.
The modal analysis of the tensegrity structure is conducted by neglecting the damping matrix and the vector of applied forces in Eq.1. The generalized eigenproblem (Eq. 8) is then obtained considering a small harmonic motion of the form: $u = \bar{u}\ sin(\omega t)$, where ω is the angular frequency and $\bar{u}$ is the amplitude vector.

$$\mathbf{K_T}\ \bar{u} = \omega^2 \mathbf{M}\ \bar{u} \qquad \text{[Eq. 8]}$$

The spectral decomposition of matrix $\mathbf{M^{-1}K}$ then yields the natural frequencies and corresponding mode shapes of the finite element model (FEM) of the structure.
Modal analysis was first performed for reference self-stress configuration of the tensegrity structure. The reference self-stress level corresponds to configuration where length of both static and active struts is equal to 1298.5mm. Results are shown in Table 1. Natural frequencies are presented for the five lowest modes in Hz.

Isometric views of the first five mode shapes are presented in Figure 4. Modal analysis results show the existence of pairs of modes with close frequencies and almost symmetrical shapes. This can be explained by the configuration of the structure. The structure is not symmetrical because of support positions and the number of basic modules. Mode shapes involve synchronous and asynchronous vertical deformation of adjacent modules. In addition, none of the modes corresponding to the first five natural frequencies can be identified clearly as a deformation mode (bending or torsion modes).

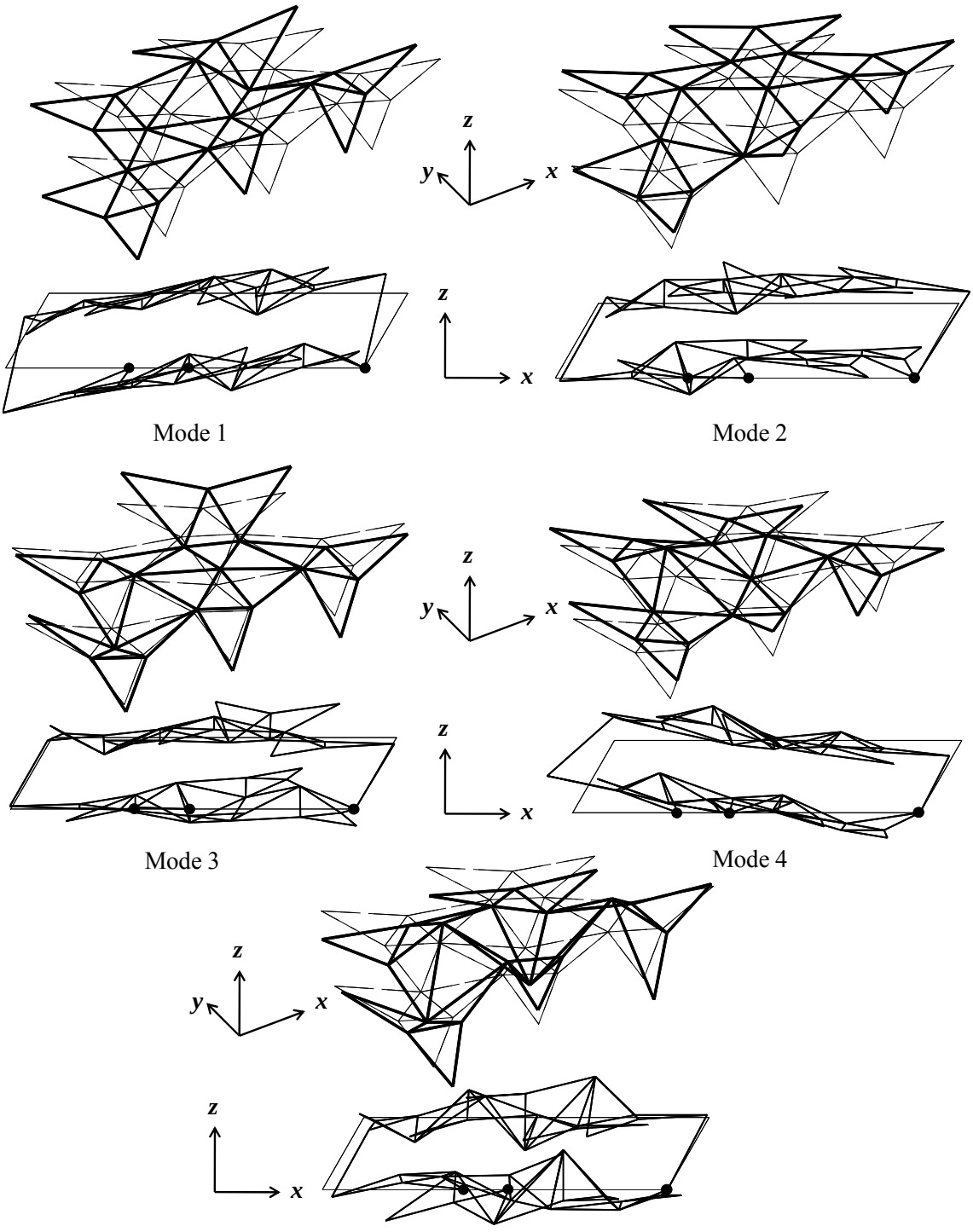

Fig. 4. Mode shapes for the first five natural frequencies.

To gain understanding of the vibrational characteristics of the tensegrity structure, the evolution of first natural frequencies is studied with respect to the self-stress level. Modal analysis is then performed with 14 self-stress configurations. These self-stress levels are obtained through making different contractions and elongations of active struts. For each configuration, the same length adjustment is applied to all active struts. For each self stress configuration, element stresses are calculated using a static analysis program based on dynamic relaxation using kinetic damping (Domer et al. 2003). Stiffness matrices are then formed and the eigenproblem is solved to obtain natural frequencies and mode shapes.

Active strut length is varied from 1295.5 to 1308.5mm by steps of 1mm. Modifying active strut lengths changes the distribution of element internal forces and affects also the geometry of the tensegrity structure. In general, when increasing active strut lengths, struts and cables experience increasing values of axial forces but in the same time geometry changes result in some slack cables. Evolution of tension in a reference cable for increasing active strut length is displayed in Figure 5. In this figure, zero elongation corresponds to the initial length of active struts (1298.5mm). Figure 6 shows the number of slack cables for different degrees of self-stress. In all cases slacking happened in cables forming the small triangle (Figure 3 and 12) and did not cause loss of stability. In this structure, module topology and module connections are designed to provide redundancy. The basic module contains more cables than required for stability. Moreover, module connection involves multiple cables and nodes. Consequently, the structure exhibits redundant load path behaviour and therefore, slackening in some cables does not compromise stability. In previous work, Adam and Smith (2007a) studied damage tolerance of the structure and identified critical elements. Elements are called critical when their rupture leads to structural collapse. Adam and Smith (2007a) showed that for the original self-stress configuration, only 10% of cables are critical. However, the number of critical cables increases when the self-stress is modified.

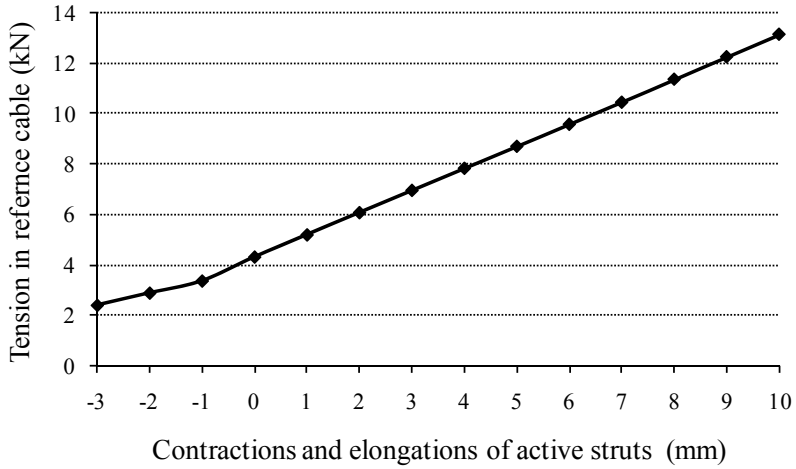

Fig. 5. Tension in a reference cable for different active strut movements.

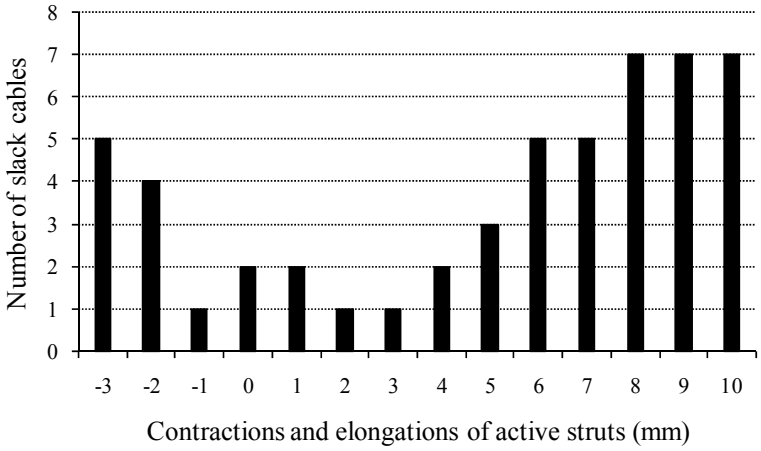

Fig. 6. Number of slack cables for different active strut movements.

Results of the modal analysis for increasing self-stress levels are shown in Figure 7. The evolution of ten first natural frequencies is studied with respect to the self-stress level of the tensegrity structure. Not surprisingly, the values of natural frequencies increase with increasing level of self-stress. Figure 7 shows that mode: 1, 2, 3, 5, 6 and 7 are significantly affected by increasing the degree of self-stress. In contrast, natural frequencies values corresponding to modes 4, 8, 9 and 10 exhibit slower increases with respect to the level of self-stress.

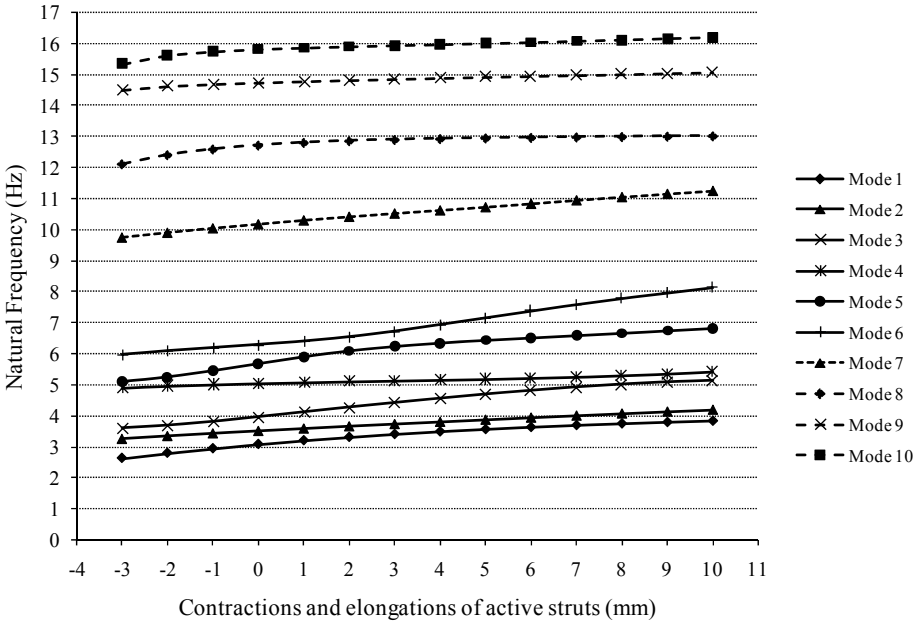

Fig. 7. First natural frequencies for different active strut movements.

The self-stress level plays a key part in providing stiffness to tensegrity structures. As shown in Eq.1, the tangent stiffness $\mathbf{K_T}$ of a tensegrity structure is constituted by the elastic stiffness $\mathbf{K_E}$, employed for small deformations truss analyses, and the geometrical stiffness $\mathbf{K_G}$, induced by pre-stresses. Consequently, when the structure experiences infinitesimal mechanisms, the elastic term vanishes and the stiffness is induced only by $\mathbf{K_G}$ (Murakami and Nishimura 2001b). This suggests that modes increasing with the level of self-stress correspond to the tensegrity infinitesimal mechanisms. Similar results had been revealed in earlier studies concerned with tensegrity dynamics. Studying a six stage tensegrity mast, Murakami (2001a; 2001b) showed that frequencies of internal mechanism modes can be increased by increasing the self-stress level. In contrast, frequencies of flexural modes, which have non-zero elastic energy, do not change significantly with the self-stress level. Moussa et al (2001) showed that the fundamental modes of simplex type modules are those corresponding to internal mechanisms and proposed a direct relation between self-stress and first natural frequency. Dubé et al (2008), for a tensegrity minigrid, as well as Tibert and Pellegrino (2003), for a deployable tensegrity mast, obtained similar results.

In the next section, laboratory tests carried out to identify the first natural frequencies of the tensegrity structure are described. Experimental modal analysis results are then compared to those obtained analytically.

4. Experimental modal analysis

4.1 Free vibration tests

Preliminary modal tests were conducted to determine the natural frequencies and mode shapes of the tensegrity structure. Free vibration tests employed a single mass that was suspended from a node on the top surface of the structure. Displacement measurements began once the load was suddenly removed. Ten tests were carried out with two initial loads at five nodes such that all modes of interest were excited. Vertical displacements were measured at 7 nodes of the top surface of the structure and standard signal processing techniques were applied to calculate frequency response functions (FRFs).

Details of initial loading, loaded nodes and measurement locations are summarized in Table 2. Examples of response recordings are shown in Figures 8 and 9. These two figures show time history of the vertical displacement of node 50 and node 39. Displacements have been measured after a load removed of 640 N at node 16. Fourier spectrums obtained from the responses are shown in Figure 10 and 11.

Analysis of the free vibration results reveals the existence of a beat phenomenon in tensegrity time history response. This observation suggests that the natural frequencies of the tensegrity structure are relatively closely spaced which confirms FEM results (Table 1). This is also confirmed by Fourier spectrums obtained from the corresponding responses. The spectra in Figure 10 indicated that the first three natural frequencies of the structure are located between 3 and 4 Hz.

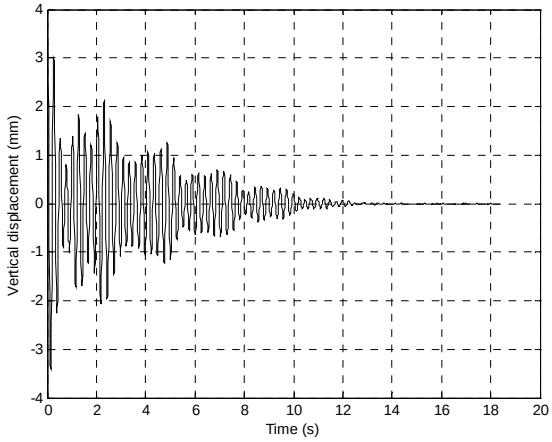

Fig. 8. Time history of vertical displacement of node 50 (640 N at node 16)

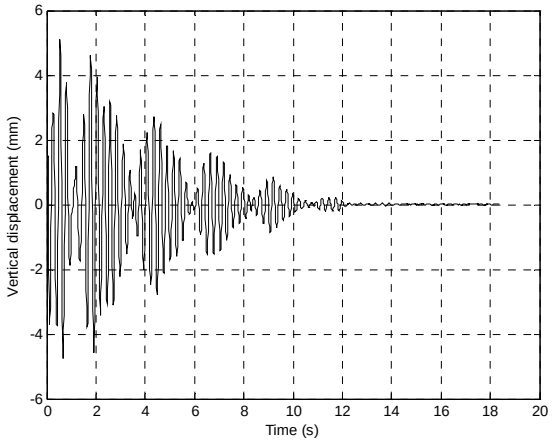

Fig. 9. Time history of vertical displacement of node 39 (640 N at node 16)

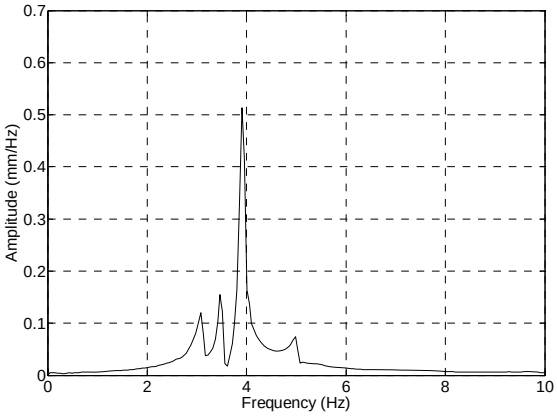

Fig. 10. Fourier amplitude spectra of vertical displacement of node 50 (640 N at node 16)

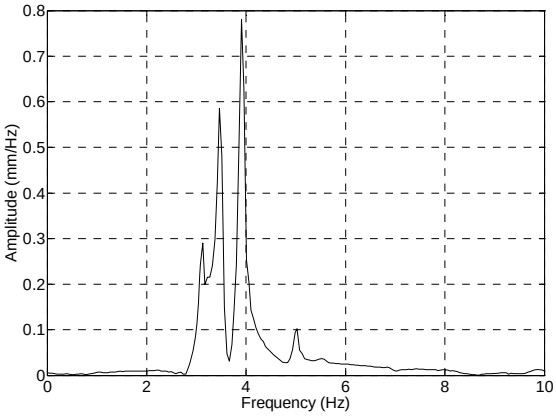

Fig. 11. Fourier amplitude spectra of vertical displacement of node 39 (640 N at node 16)

Modal identification analysis of the tensegrity structure was performed using the Frequency Domain Decomposition technique (FDD). The FDD technique consists of decomposing the system response into a set of single degree of freedom systems, each corresponding to an individual mode, through a decomposition of the spectral density function matrix (Brincker et al. 2001). The modal damping ratios can be estimated using an enhanced version of the FDD method, the EFDD method. The first structural modes of the tensegrity structure are easily identified. Natural frequencies as well as damping ratios for the first five modes are displayed in Table 3. Table 3 also gives values for the standard deviations for frequency and damping.

Experimentally identified natural frequencies are compared with those determined by the FEM (Table 1). Experimental and analytical results match within a few percent for the first five natural frequencies. Therefore, the linearized dynamic model offers a good approximation of the nonlinear behavior of the five modules tensegrity structure. The experimental and analytical studies indicated closely spaced natural frequencies (the beat

phenomenon) which in general may prevent an accurate determination of modal characteristics through identification techniques (Brincker et al. 2001). Additional experimental investigations including forced vibration experiments are thus carried out. In the next section, forced vibration tests are described. Results are then compared to those obtained analytically and through free vibration tests in order to get more information about the tensegrity structure.

4.2 Forced vibration tests

Experimental modal analysis of the tensegrity structure through free vibrations is completed by vibration experiments. Forced vibrations were conducted to determine natural frequencies and damping characteristics for different self-stress level of the tensegrity structure. Testing involved exciting the tensegrity structure and measuring the vibration response. The shaker used to excite the structure in this study was an electro-mechanic device composed of an electric motor connected to a linearly activated mass. The shaker was connected to a signal amplifier in order to control the excitation frequencies. For all tests the shaker was connected to node 43 and vertical displacement measurements were taken at the top surface nodes of the structure.
Vibration tests were performed for different self-stress level in order to identify the relationships between the pretension level of the tensegrity structure and its dynamic behavior. The tensegrity self-stress level was controlled through elongations and contractions of active struts. In addition to the initial self-stress configuration taken to be zero elongation, ten self-stress states were studied. These self-stress states were obtained through making six different contractions of active struts (form 0.5 to 3mm) as well as four elongations (from 0.5 to 2mm) by steps of 0.5mm. For each self-stress level, elongations or contractions were made simultaneously for all active struts. The evolution of average internal forces in different element of the structure and the number of slack cables are given in Table 4. The basic module cables are divided into big triangle cables, small triangle cables and lateral cables (Figure 12).

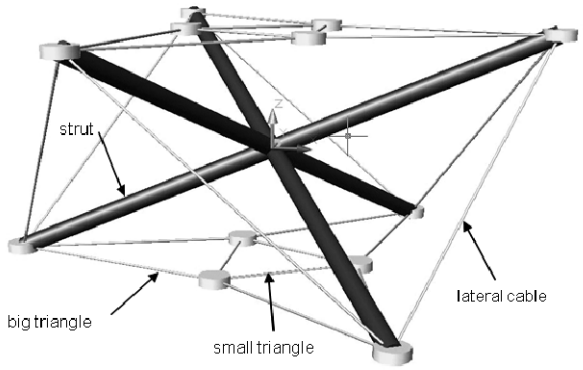

Fig. 12. Basic module of the tensegrity structure.

The relationship between the dynamic response and the self-stress level of the tensegrity structure has been studied experimentally. Excitation tests have been performed with frequencies running between 1.5 and 4.0 Hz. Figure 13 illustrates the variation of the tensegrity response amplitude at node 39 according to the excitation frequencies and self-stress level. Amplitude peaks in Figure 13 correspond to the first resonance frequencies of the structure for the self-stress levels that were studied. Stress levels are varied around a reference stress (Ref) through increments of millimeter elongations and contractions. For example, (Ref+1) denotes the stress level induced by a one mm elongation of active struts from the reference stress level. The first natural frequencies for the different self-stress levels are easily identified. Figure 13 shows that amplitude peaks change with respect to self-stress level. Decreasing active strut lengths has the effect of reducing the natural frequency of the first resonance mode. Moreover, it is shown that the maximum amplitude is modified when the first vibration mode is shifted in frequency by acting on active struts. These results suggest that modifying the self-stress level of the tensegrity is not only affecting the stiffness of the structure but also damping characteristics. These results confirm that, as observed for other configurations, the dynamic response of this tensegrity structure is closely related to its self-stress level.

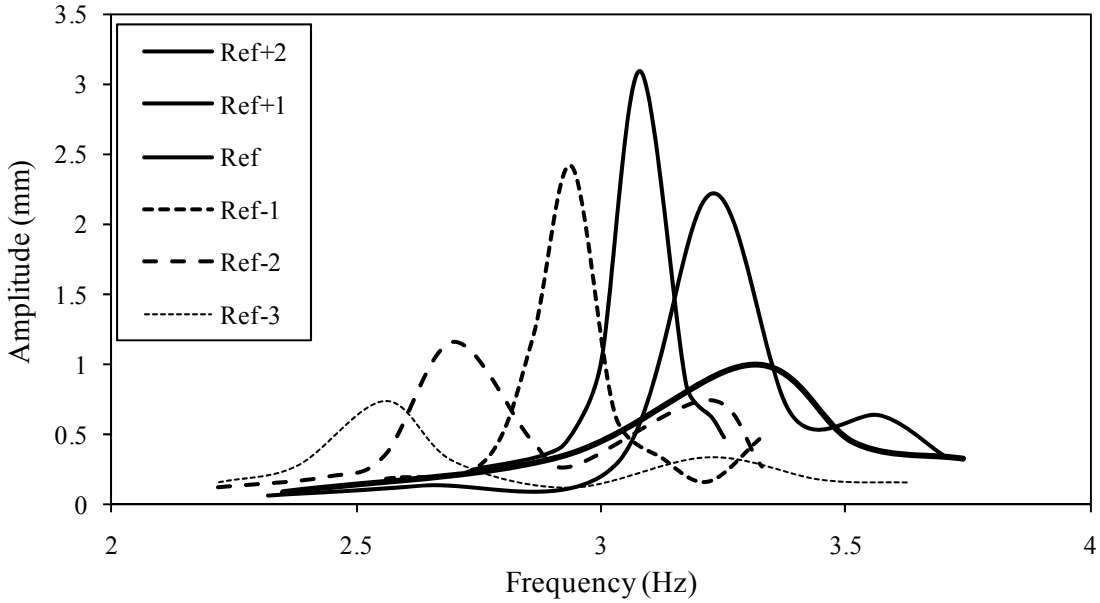

Fig. 13. Vibration amplitude at node 39 for different excitation frequencies and stress levels.

The first natural frequency of the structure with the Ref self-stress level is about 3.08 Hz. This matches well with the experimental modal analysis results presented earlier (3.07 Hz). The evolution of the first natural frequency of the structure with respect to the degree of self-stress is displayed in Figure 14. It is shown that experimental and analytical results match well for the different self-stress levels.

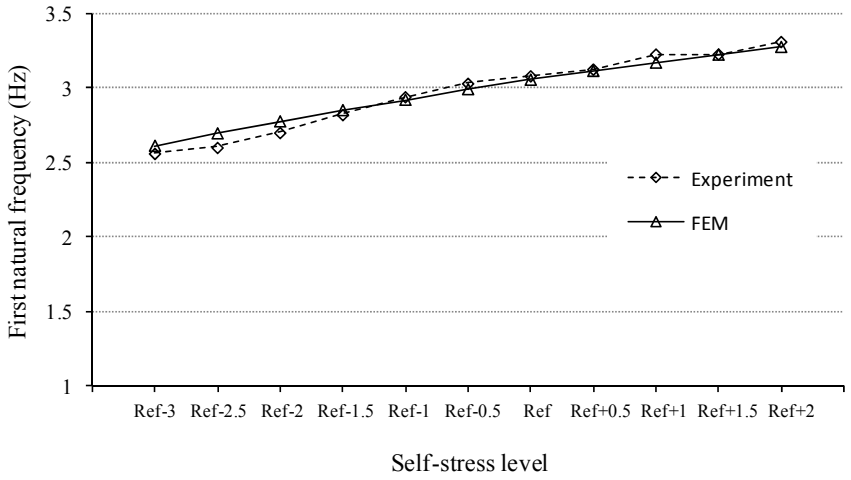

Fig. 14. Evolution of the first natural frequency with respect to self-stress level.

Vibration experiments are also employed to estimate the damping ratio of the first vibration mode for the studied self-stress levels. Estimated values of damping ratios with respect to the degree of self-stress are displayed in Figure 15. The damping ratio associated with the first vibration mode of the structure when active struts are in their reference position is estimated to be 1.65%. This result contrasts with the damping estimation given by the EFDD method (Table 3). It is conjectured that such discrepancy arises because of the closely spaced natural frequencies. Vibration experiments showed also that the damping is amplitude-dependent and this hinders evaluation and comparison with results obtained with free vibration testing. The damping ratios calculated using both methods should thus be considered as rough estimations. Figure 15 shows also that the damping ratio increases when the self-stress level in the tensegrity structure decreases. The increase in modal damping may be caused by increasing friction in the joints. Slack cables can also be a source of energy dissipation. These results show that, in parallel with natural frequencies, the tensegrity damping characteristics can be tuned by varying the level of self-stress.

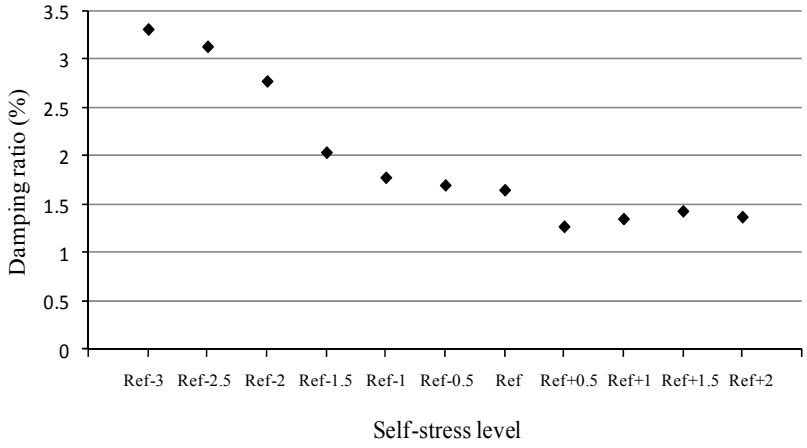

Fig. 15. Evolution of the damping ratio with respect to self-stress level.

5. Vibration control

Experimental measurements and numerical simulations have confirmed that the dynamic behavior of the five module active tensegrity structure is closely related to its degree of self-stress. These results indicate the potential to adjust the natural frequencies of the structure to meet vibration control requirements. Under a given excitation loading, response amplitudes may be attenuated through shifting natural frequencies away from the excitation. This can be carried out by modifying the self-stress level of the tensegrity structure through active strut movements.

A general objective of vibration control is to reduce structural response resulting from initial disturbances to acceptable levels with a minimum control cost. Active struts of the structure can be elongated or contracted, changing the self-stress level, thereby modifying natural frequencies of the system. The vibration control objective of the tensegrity structure is formulated as follows: find a set of strut positions defining a self-stress level configuration that shifts the natural frequencies away from a given excitation frequency. In addition, it is important to achieve this objective in an optimal manner leading to least perturbation of the geometry and the stiffness of the structure.

The vibration control task can thus be stated as an optimization problem where the objective function measures the distance between the excitation frequency and the nearest natural frequency of the structure under a particular self-stress level.
Let $\mathbf{x}^{\mathbf{t}} = [x_1, x_2, ..., x_{10}]$ be the vector of active strut movements. The vibration control problem can be stated as follows:

$$Max\ F_1(x) = \left| f_n(x) - f_{ex} \right| \qquad \text{[Eq. 9]}$$

Subject to

$$g_{x,\max} = x_{i,\max} - x_i \geq 0, \qquad \forall i = 1,...,10 \qquad \text{[Eq. 10]}$$

$$g_{x,\min} = x_i - x_{i,\min} \geq 0, \qquad \forall i = 1,...,10 \qquad \text{[Eq. 11]}$$

Where f_{ex} is the excitation frequency and f_n is the nearest resonance frequency of the structure to excitation frequency. Natural frequencies are calculated under current self-stress level defined after applying active strut adjustments. Equation 10 and 11 represent the constraints on the decision variable values. We assume that each active strut adjustment x_i is limited to values running between $x_{i,\ min}$ and $x_{i,\ max}$.

The number of active struts and the discrete strut moves define the space of possible solutions. With ten active struts, it is impossible to generate and test every possible solution due to the combinatorial nature of the task. Stochastic search is therefore useful for this situation. Stochastic methods sample the solution space using special strategies. Although

there is no guaranty of reaching a global optimum, near optimal solutions are usually sufficient for control applications.
This optimization task was addressed using Probabilistic Global Search Lausanne (PGSL). The PGSL technique is based on the assumption that sets of better solutions are more likely to be found in the neighborhood of sets of good solutions and, therefore, intensifies search in regions that contain sets of good values. Search is driven by probability density functions (Raphael and Smith 2003). Preliminary numerical tests have revealed that many combinations of contractions and elongations of active struts can satisfy the control objective to an acceptable degree. Vibration control can then be enhanced considering a multi-objective approach instead of the single objective function formulated in Eq.9.

Assuming that varying the self-stress level causes perturbation of geometry and stiffness of the tensegrity structure, a robust approach seems to be more appropriate for the vibration control problem. This means that the solution requires the minimization of a second objective function where the control cost is taken into consideration. Control cost is evaluated through the sum of active strut adjustments which has to be minimized. This is a simple manner to guaranty that vibration control will be done with least perturbation of both geometry and stiffness of the tensegrity structure. A second objective function is then formulated (Eq.12).

$$F_2(x) = \sum_{i=1}^{10} x_i^2 \qquad \text{[Eq. 12]}$$

As a multi-objective problem, vibration control requires the generation of a set of possible solutions, defined as those able to satisfy best and with different performances the two objectives defined in Eq.9 and 12. These solutions are known as Pareto optimal or non-dominated solutions. In a multi-objective minimization task, a solution x^* is said to be Pareto optimal if no feasible vector of decision variables can be found that improves values for any objective function without causing a simultaneous increase in other objectives. The solution is then selected between mutually non-dominated candidates. However, in the absence of preference information, none of the Pareto optimal solutions could be said to be better than the others.

Recent advances in multi-objective optimization resulted in reliable techniques for generating non-dominated solutions. Evolutionary techniques are currently used in various fields due to their effectiveness and robustness in searching for a set of trade-off solutions (Coello Coello et al. 2007). However, the selection of the "best solution" to be adopted among the Pareto optimum set is a challenge. Several decision support systems have recently been proposed to help in the selection of the best compromise alternatives. Major approaches to Multi-Criteria Decision Making (MCDM) include multi-attribute utility theory and outranking methods (Coello 2000). Incorporating preferences is also considered to help in handling conflicting objectives (Fleming et al. 2005). Adam and Smith (2007b) proposed and validated experimentally a multi-objective approach to compute control commands for quasi-static control of tensegrity structures. The search method is based on

building a Pareto optimal solution set. A hierarchical selection strategy is then adopted to reduce the solution space until identification of a control command. Grierson (2008) proposed a MCDM strategy employing a tradeoff-analysis technique to identify compromise designs for which the competing criteria are mutually satisfied in a Pareto optimal set.

In this study, the methodology for multi-objective vibration control includes two phases. First, the multi-objective problem is solved using PGSL optimization. A set of solutions is generated and then filtered so that only Pareto optimal solutions are considered. Second, an outranking relation is employed to select a compromise control solution. Outranking is performed using the PROMETHEE method (Preference Ranking Organization METHod for Enrichment Evaluation) (Brans and Mareschal 2005). The PROMETHEE method was developed as a MCDM method to solve discrete decision problems with conflicting criteria.

In the PROMETHEE method, a preference index is used to compute a net flow for each Pareto optimal solution. This value is then used to rank the Pareto optimal set.
Let S_1, S_2, ... S_i, ... S_n be n Pareto optimal solutions and f_1, f_2, … f_k, … f_m denote the m objective functions. The preference flow for each solution is formulated as follows:

$$\phi\ (S_i) = \phi^+(S_i) - \phi^-(S_i) \qquad \text{[Eq. 13]}$$

$$\varphi^+(S_i) = \sum_{j=1}^{m} C(S_i, S_j) \qquad \text{[Eq. 14]}$$

$$\varphi^-(S_i) = \sum_{j=1}^{m} C(S_j, S_i) \qquad \text{[Eq. 15]}$$

The preference index $C(S_i, S_j)$ is defined in Eq.16, where w_k are weights expressing the relative importance of the decision criteria.

$$C(S_i, S_j) = \sum_{k=1}^{n} w_k . P_k(S_i, S_j) \Big/ \sum_{k=1}^{n} w_k \qquad \text{[Eq. 16]}$$

Brans and Mareschal (2005) proposed six types of preference functions $P_k(S_i, S_j)$ used to express the intensity of preference. Through these functions, indifference or gradual degrees of preference are associated to the deviations observed between the evaluations of two solutions.
Control command computation is presented for a particular excitation case loading. Experimental tests are also presented to show the effectiveness of the vibration control algorithm.

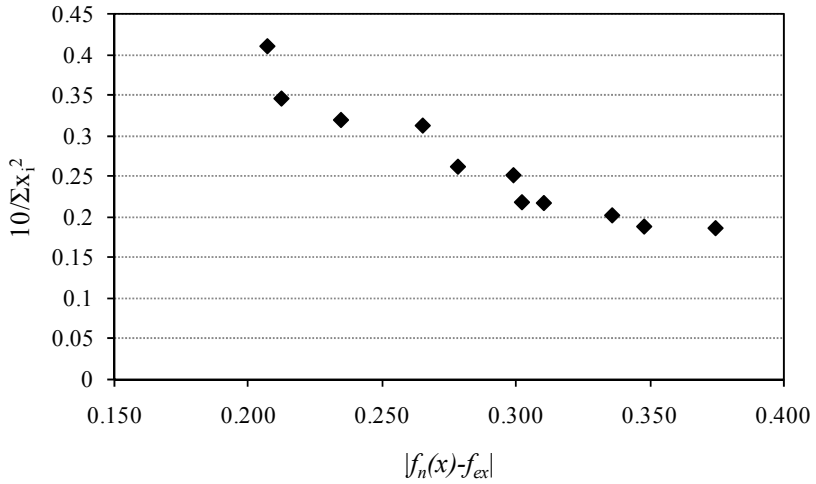

Fig. 16. Pareto optimal solutions.

A 3 Hz excitation force was applied to node 43 to excite the structure. The frequency of the excitation force was selected to be close to the first natural frequency of the tensegrity structure. Active strut movements were limited to ± 3 mm and the precision range of each move in steps of ± 0.1 mm. Control solutions are found through optimization employing the PGSL algorithm. For this purpose, the first objective function (F_1) is optimized while the second objective function F_2 is transformed into inequality constraint (Eq.17).

$$F_2(x) = \sum_{i=1}^{10} x_i^2 \leq \varepsilon \qquad \text{[Eq. 17]}$$

By changing the bound ε of the new constraint, we obtained 30 solutions of our problem using the PGSL algorithm. Dominated solutions were eliminated and only eleven solutions are considered in the Pareto optimum set. Pareto optimal solutions are presented in Figure 16 with respect to the two objectives. It must be pointed out that, the arbitrary choice of values for ε didn't allow us to obtain a good spread of solutions on the Pareto curve in Figure 16. However, the methodology adopted here resulted in a sufficient number of solutions meeting with control requirements.

The PROMETHEE II method was then applied using linear preference functions (Eq.18 and 19) and the same weight (w_1=w_2=1) is considered for the two objective functions.

$$P_1(S_i, S_j) = \begin{cases} 0 & \text{if } F_1(S_i) \leq F_1(S_j) \\ (F_1(S_i) - F_1(S_j)) \big/ (F_1^{\max} - F_1^{\min}) & \text{if } F_1(S_i) > F_1(S_j) \end{cases} \qquad \text{[Eq. 18]}$$

$$P_2(S_i, S_j) = \begin{cases} 0 & \text{if } F_2(S_i) \geq F_2(S_j) \\ (F_2(S_i) - F_2(S_j)) \big/ (F_2^{\min} - F_2^{\max}) & \text{if } F_2(S_i) < F_2(S_j) \end{cases} \qquad \text{[Eq. 19]}$$

The preference flow is calculated for each solution of the Pareto optimal set and a complete preorder is established (Table 5). According to the results showed in Table 5, solution S4 has the highest preference flow value (1.599) and thus can be preferred to all other solutions. S6 comes in the second place with a positive preference flow value of 0.907. These results are compared to those of PEG–MCDM procedure proposed by Grierson (2008). The PEG–MCDM procedure defines a unique compromise design for which all the criteria are mutually satisfied in a Pareto-tradeoff sense. Using the PEG–MCDM procedure for the vibration control problem, the Pareto-compromise solution mutually agreeable for both objectives is a control solution with $F_1 = 0.29$ and $F_2 = 39.21$. This is a Pareto optimal solution very close to the solution S_6 in Table 5. The control solution identified through PROMETHEE II outranking strategy with linear preference functions and considering the same weight for the two objective functions is different from the Pareto-competitive equilibrium point identified using PEG-MCDM procedure. This suggests that a compromise solution with mutually agreeable objectives is not necessarily the preferred solution using a preference-based outranking strategy.

The control solution (S_4) was applied to the tensegrity structure for experimental validation. Figure 17 shows the time history of the vertical displacement at node 39 for controlled and uncontrolled configurations. Displacement amplitude is reduced by 90% after control. The vibration amplitude at node 39 for uncontrolled configuration is about 2.6mm. The application of the control command on the structure by adjusting lengths of the ten active struts of the structure took less than 40 seconds. Note that controlling the structure results in geometry changes leading node 39 to move 1.9mm away from its initial position. Vertical displacements caused by control application are less than 5mm for all structure nodes and for element internal forces vibration control results in a maximum variation of about 17%.

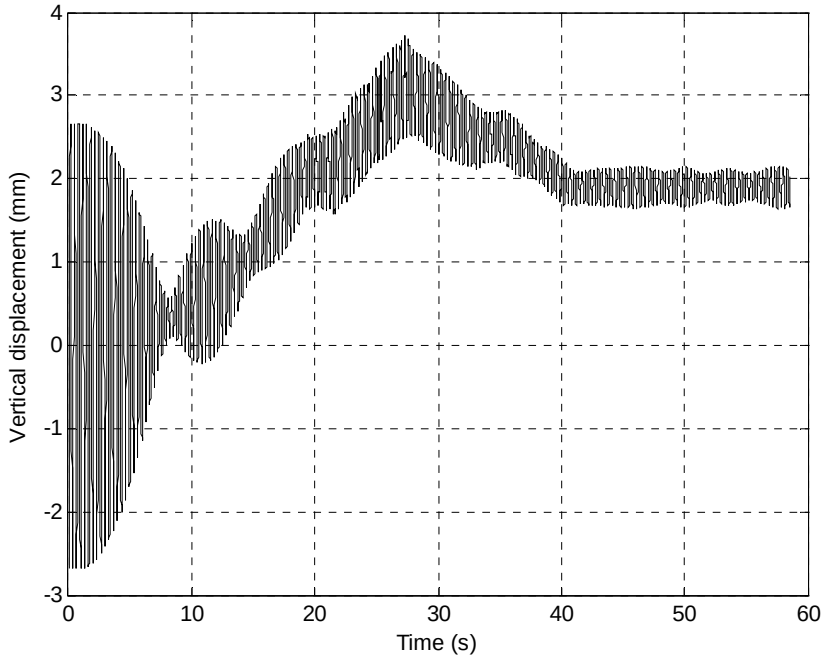

Fig. 17. Vertical displacement of node 39 for controlled and uncontrolled configurations.

6. Limitations and Future work

Laboratory tests showed the capacity of the active control system to attenuate vibrations of the five modules tensegrity structure. Vibration control strategy is based on modifying the self-stress level of the structure through contractions and elongations of active struts in order to shift the natural frequencies away from excitation. Experimental measurements and numerical simulations showed that unlike infinitesimal modes, the frequencies of deformation modes (flexural and torsion modes) does not change significantly with the self-stress level of the tensegrity structure. This observation suggests that the proposed vibration control strategy is particularly useful when internal mechanism vibration modes are excited.

Control results demonstrate the ability of both stochastic search through PGSL and an outranking MCDM strategy to find good control solutions. Since many combinations of contractions and elongations of active struts satisfy the vibration damping objective to an acceptable degree, additional robustness objectives might be taken into consideration. Control performance can also be improved using reinforcement learning. Adam and Smith (2007b) showed that memorizing, retrieving and adapting previous control events improves shape control of active tensegrity structure.

Further challenges, such as considering more complex dynamic loading that are representative of practical situations have been identified. Moreover, a change in mass distribution can be considered to simulate variable loading in real cases. As shown in this

study, a linearized dynamic model offers a good approximation of the nonlinear behavior of the five modules tensegrity structure. However, generalization to other structures requires implementation of additional numerical algorithms and modeling techniques.

7. Conclusion

Active tensegrity structures are reusable structural systems that are capable of reacting to their environment. In this paper, we focus on the dynamic behavior and the vibration control of a five module active tensegrity structure. The control strategy adopted in this tensegrity structure is capable of meeting vibration control objectives. Experimental as well as numerical results confirmed that natural frequencies can be shifted when the self-stress level in the tensegrity structure is modified. Vibration control is formulated as a multi-objective optimization problem. Control commands are identified using stochastic search through PGSL and PROMETHEE outranking strategy. The capacity of the active control system to attenuate vibrations by shifting values of natural frequencies away from excitation is demonstrated. These results are expected to provide further progress leading to more robust adaptive civil engineering structures.

Acknowledgements
The authors would like to thank the Swiss National Science Foundation for supporting this work (FN Grant no 200020-121552/1). E. Fest, B. Domer, B. Adam are recognized for building the structure and the quasi-static control system. Dr. Clotaire Michel is thanked for discussion and advice. We are also grateful to S. Demierre and P. Gallay for their contributions.

References

Adam, B. (2007). "Adaptive civil engineering structures: the example of tensegrity," PhD Thesis N° 3750, Ecole Polytechnique Fédérale de Lausanne, Switzerland.

Adam, B., and Smith, I. F. C. (2007a). "Self-Diagnosis and Self-Repair of an Active Tensegrity Structure." *Journal of Structural Engineering*, 133(12), 1752-1761.

Adam, B., and Smith, I. F. C. (2007b). "Tensegrity Active Control: Multiobjective Approach." *Journal of Computing in Civil Engineering*, 21(1), 3-10.

Arsenault, M., and Gosselin, C. M. (2006). "Kinematic, Static, and Dynamic Analysis of a Spatial Three-Degree-of-Freedom Tensegrity Mechanism." *Journal of Mechanical Design*, 128(5), 1061-1069.

Averseng, J., and Crosnier, B. (2004). "Static and dynamic robust control of tensegrity systems." *Journal of The International Association for Shell and Spatial Structures*, 45(146), 169-174.

Barnes, M. R. (1999). "Form Finding and Analysis of Tension Structures by Dynamic Relaxation." *International Journal of Space Structures*, 14, 89-104.

Ben Kahla, N., Moussa, B., and Pons, J. C. (2000). "Nonlinear dynamic analysis of tensegrity systems." *Journal of The International Association for Shell and Spatial Structures*, 41(132), 49-58.

Brans, J.-P., and Mareschal, B. (2005). "Promethee Methods." Multiple Criteria Decision Analysis: State of the Art Surveys, 163-186.

Brincker, R., Zhang, L., and Andersen, P. (2001). "Modal identification of output-only systems using frequency domain decomposition." *Smart Materials and Structures*, 10(3), 441-445.

Carstens, S., and Kuhl, D. (2005). "Non-Linear Static and Dynamic Analysis of Tensegrity Structures by Spatial and Temporal Galerkin Methods." *Journal of the International Association for Shell and Spatial Structures*, 46(2), 116-134.

Chan, W., Arbelaez, D., Bossens, F., and Skleton, R. E. (2004). "Active vibration control of a three-stage tensegrity structure." SPIE 11th Annual International Symposium on Smart Structures and Materials, San Diego, California, USA.

Coello, C. A. C. "Handling preferences in evolutionary multiobjective optimization: a survey." *Evolutionary Computation, 2000. Proceedings of the 2000 Congress on*, 30-37 vol.1.

Coello Coello, C. A., Lamont, G. B., and Van Veldhuizen, D. A. (2007). *Evolutionary Algorithms for Solving Multi-Objective Problems*, Springer US.

de Jager, B., and Skelton, R. E. (2005). "Input-output selection for planar tensegrity models." *Control Systems Technology, IEEE Transactions on*, 13(5), 778-785.

Djouadi, S., Motro, R., Pons, J. C., and Crosnier, B. (1998). "Active Control of Tensegrity Systems." *Journal of Aerospace Engineering*, 11(2), 37-44.

Domer, B., Fest, E., Lalit, V., and Smith, I. F. C. (2003). "Combining Dynamic Relaxation Method with Artificial Neural Networks to Enhance Simulation of Tensegrity Structures." *Journal of Structural Engineering*, 129(5), 672-681.

Domer, B., and Smith, I. F. C. (2005). "An Active Structure that Learns." *Journal of Computing in Civil Engineering*, 19(1), 16-24.

Dubé, J. F., Angellier, N., and Crosnier, B. (2008). "Comparison between experimental tests and numerical simulations carried out on a tensegrity minigrid." *Engineering Structures*, 30(7), 1905-1912.

Fest, E., Shea, K., and Smith, I. F. C. (2004). "Active Tensegrity Structure." *Journal of Structural Engineering*, 130(10), 1454-1465.

Fleming, P. J., Purshouse, R. C., and Lygoe, R. J. (2005). "Many-Objective Optimization: An Engineering Design Perspective." Evolutionary Multi-Criterion Optimization, 14-32.

Furuya, H. (1992). "Concept of Deployable Tensegrity Structures in Space Application." *International Journal of Space Structures*, 7(2), 143-151.

Ganesh Raja, M., and Narayanan, S. (2007). "Active control of tensegrity structures under random excitation." *Smart Materials and Structures*, 16, 809-817.

Grierson, D. E. (2008). "Pareto multi-criteria decision making." *Advanced Engineering Informatics*, 22(3), 371-384.

Guest, S. (2006). "The stiffness of prestressed frameworks: A unifying approach." *International Journal of Solids and Structures*, 43(3-4), 842-854.

Kanchanasaratool, N., and Williamson, D. (2002). "Modelling and control of class NSP tensegrity structures." *International Journal of Control*, 75, 123-139.

Kebiche, K., Kazi-Aoual, M. N., and Motro, R. (1999). "Geometrical non-linear analysis of tensegrity systems." *Engineering Structures*, 21(9), 864-876.

Kono, Y., Choong, K. K., Shimada, T., and Kunieda, H. (1999). "An experimental investigation of a type of double-layer tensegrity grids " *Journal of the International Association for Shell and Spatial Structures*, 40(130), 103-111.

Masic, M., and Skelton, R. E. (2006). "Selection of prestress for optimal dynamic/control performance of tensegrity structures." *International Journal of Solids and Structures*, 43(7-8), 2110-2125.

Mirats Tur, J. M., and Juan, S. H. (2009). "Tensegrity frameworks: Dynamic analysis review and open problems." *Mechanism and Machine Theory*, 44(1), 1-18.

Motro, R. (2003). *Tensegrity: Structural systems for the future*, U.K.

Motro, R., Najari, S., and Jouanna, P. (1986). "Static and Dynamic Analysis of Tensegrity Systems." ASCE International Symposium on Shells and Spatial Structures, Computational Aspects, Springer, ed., New York, NY, USA, 270-279.

Moussa, B., Ben Kahla, N., and Pons, J. C. (2001). "Evolution of Natural Frequencies in Tensegrity Systems: A Case Study." *International Journal of Space Structures*, 16, 57-73.

Murakami, H. (2001a). "Static and dynamic analyses of tensegrity structures. Part 1. Nonlinear equations of motion." *International Journal of Solids and Structures*, 38(20), 3599-3613.

Murakami, H. (2001b). "Static and dynamic analyses of tensegrity structures. Part II. Quasi-static analysis." *International Journal of Solids and Structures*, 38(20), 3615-3629.

Murakami, H., and Nishimura, Y. (2001a). "Static and dynamic characterization of regular truncated icosahedral and dodecahedral tensegrity modules." *International Journal of Solids and Structures*, 38(50-51), 9359-9381.

Murakami, H., and Nishimura, Y. (2001b). "Static and Dynamic Characterization of Some Tensegrity Modules." *Journal of Applied Mechanics*, 68(1), 19-27.

Oppenheim, I. J., and Williams, W. O. (2001a). "Vibration and Damping in Three-Bar Tensegrity Structure." *Journal of Aerospace Engineering*, 14(3), 85-91.

Oppenheim, I. J., and Williams, W. O. (2001b). "Vibration of an elastic tensegrity structure." *European Journal of Mechanics - A/Solids*, 20, 1023-1031.

Paronesso, A., and Passera, R. (2004). "The cloud of Yverdon." IASS 2004 Symposium, International Association for Shell and Spatial Structures, Editions de l'Espérou, Montpellier.

Raphael, B., and Smith, I. F. C. (2003). "A direct stochastic algorithm for global search." *Applied Mathematics and Computation*, 146(2-3), 729-758.

Sultan, C., Corless, M., and Skelton, R. E. (2002). "Linear dynamics of tensegrity structures." *Engineering Structures*, 24(6), 671-685.

Tan, G. E. B., and Pellegrino, S. (2008). "Nonlinear vibration of cable-stiffened pantographic deployable structures." *Journal of Sound and Vibration*, 314(3-5), 783-802.

Tibert, A. G., and Pellegrino, S. (2003). "Deployable tensegrity mast." 44th AIAA/ASME/ASCE/AHS/ASC, Structures, Structural Dynamics and Materials Conference and Exhibit, Norfolk , VA, USA.

Tables

Table 1: FEM Natural frequencies of the tensegrity structure

Mode	Frequency (Hz)
Mode 1	3.056
Mode 2	3.484
Mode 3	3.947
Mode 4	5.027
Mode 5	5.658

Table 2: Loading for free vibration testing

Load (N)	Loaded nodes	Measured nodes
400	16, 34, 37, 43, 48	50, 34, 51, 41, 45, 16, 39
640	16, 34, 37, 43, 48	50, 34, 51, 41, 45, 16, 39

Table 3: Natural frequencies and corresponding damping ratios of the tensegrity structure

Mode	Natural frequencies		Damping	
	Frequency [Hz]	Standard deviation [Hz]	Damping Ratio [%]	Standard deviation [%]
Mode 1	3.07	0.009	2.63	0.261
Mode 2	3.51	0.006	1.60	0.285
Mode 3	3.91	0.008	1.40	0.081
Mode 4	5.02	0.013	2.30	0.185
Mode 5	5.67	0.010	1.19	0.285

Table 4: Self-stress levels studied for the tensegrity structure

Self-stress level	Active strut adjustment (mm)	Average internal force (N)				Slack cables
		Struts	Lateral cables	Big triangle cables	Small triangle cables	
Ref -3	-3	-10130.5	2907.2	3746.7	853.0	5
Ref -2.5	-2.5	-10824.4	3117.6	3998.7	910.5	5
Ref -2	-2	-11532.0	3332.3	4255.7	969.0	4
Ref -1.5	-1.5	-12263.0	3553.9	4521.2	1029.7	2
Ref -1	-1	-13012.8	3781.4	4793.6	1091.6	1
Ref-0.5	-0.5	-13786.2	4016.0	5074.5	1155.7	1
Ref	0	-14567.6	4253.0	5358.3	1220.3	2
Ref+0.5	+0.5	-15353.9	4491.5	5643.9	1285.3	2
Ref+1	+1	-16142.9	4730.8	5930.5	1350.5	2
Ref+1.5	+1.5	-16938.7	4972.1	6219.7	1416.2	1
Ref+2	+2	-17739.6	5215.0	6510.7	1482.2	1

Table 5: Outranking solutions of the Pareto Optimum set

Solution	$\lvert f_n(x) - f_{ex} \rvert$	$\sum_{i=1}^{10} x_i^2$	$\phi^+(S_i)$	$\phi^-(S_i)$	$\phi\ (S_i)$	Ranking
S_1	0.207	24.34	5.950	5.313	0.638	3
S_2	0.212	28.89	4.435	5.152	-0.716	8
S_3	0.234	31.27	3.972	4.118	-0.146	5
S_4	0.265	31.96	4.330	2.731	1.599	1
S_5	0.278	38.16	3.169	3.024	0.144	4
S_6	0.299	39.77	3.461	2.554	0.907	2
S_7	0.302	45.85	2.540	3.701	-1.161	10
S_8	0.310	46.05	2.855	3.552	-0.697	7
S_9	0.336	49.51	3.721	4.037	-0.316	6
S_{10}	0.348	53.14	4.117	5.006	-0.889	9
S_{11}	0.375	53.74	5.687	5.050	0.638	3

This work is licensed under a Creative Commons Attribution-NonCommercial-NoDerivatives 4.0 International License